NeuroImage 55 (2011) 1617–1632

Contents lists available at ScienceDirect

NeuroImage

journal homepage: www.elsevier.com/locate/ynimg

Robustness of intrinsic connectivity networks in the human brain to the presence of acoustic scanner noise

Dave R.M. Langers *, Pim van Dijk

Department of Otorhinolaryngology/Head and Neck Surgery, University Medical Center Groningen, The Netherlands
Faculty of Medical Sciences, School of Behavioral and Cognitive Neurosciences, University of Groningen, The Netherlands

ARTICLE INFO

Article history:
Received 26 August 2010
Revised 6 January 2011
Accepted 8 January 2011
Available online 19 January 2011

Keywords:
Functional magnetic resonance imaging (fMRI)
Acoustic scanner noise
Central auditory system
Default mode network
Intrinsic connectivity networks
Resting state

ABSTRACT

Evoked responses in functional magnetic resonance imaging (fMRI) are affected by the presence of acoustic scanner noise (ASN). Particularly, stimulus-related activation of the auditory system and deactivation of the default mode network have repeatedly been shown to diminish. In contrast, little is known about the influence of ASN on the spontaneous fluctuations in brain activity that are crucial for network-related neuroimaging methods like independent component analysis (ICA) or functional and effective connectivity analysis (ECA). The present study assessed the robustness of intrinsic connectivity networks in the human brain to the presence of ASN by comparing 'silent' (sparse) and 'noisy' (continuous) acquisition schemes, both during task performance and during rest. In agreement with existing literature, ASN strongly diminished conventional evoked response levels. In contrast, ICA and ECA robustly identified similar functional networks regardless of the scanning method. ASN affected the strength of only few independent components, and effective connectivity was hardly sensitive to ASN overall. However, unexpectedly, ICA revealed notable differences in the underlying neurodynamics. In particular, low-frequency network oscillations dominated in the commonly used continuous scanning environment, but signal spectra were significantly flatter during the less noisy sparse scanning runs. We tentatively attribute these differences to the ubiquitous influence of ASN on alertness and arousal.

Introduction

Many studies have characterized the influence of the acoustic environment on various types of processing in the human brain. In the context of neuroimaging research, the confounding effect of the loud acoustic scanner noise (ASN) that occurs during gradient switching in functional magnetic resonance imaging (fMRI) has received particular attention (Bandettini et al., 1998; Talavage et al., 1999; Amaro et al., 2002; Moelker and Pattynama, 2003). It has repeatedly been shown that blood oxygenation level dependent (BOLD) activation contrasts in response to sound stimuli typically decrease throughout the auditory system, due to a combination of elevated baseline activity and saturated hemodynamic responses (Scarff et al., 2004; Langers et al., 2005b; Gaab et al., 2007). Furthermore, other brain systems that are not nominally involved in sound processing can be affected by ASN, including those related to vision (Zhang et al., 2005), motion (Cho et al., 1998; Fuchino et al., 2006), nociception (Boyle et al., 2006), working memory (Tomasi et al., 2005), or the default mode network (Gaab et al., 2008).

So far, the effects of ASN were studied exclusively in the context of task-related responses. In recent years, novel experimental designs have been developed for fMRI that do not rely on controlled task performance, enabling measurement during diverse paradigms, naturalistic behavior, or rest. This development has been made possible by the emergence of multivariate analysis techniques that do not require prior models of stimulus-evoked brain activity. As a case in point, one may consider the numerous measures related to functional and effective brain connectivity (Friston, 1994; Horwitz et al., 2005; Rogers et al., 2007; Cole et al., 2010). These methods typically operate by identifying similarities in the functional dynamics of large sets of voxels or multiple regions of interest (ROIs). Observed covariations can arise as a result of joint responses to imposed stimuli or tasks, but may likewise emerge when interacting brain regions react to each other's spontaneous activity.

Functional and effective connectivity methods have consistently revealed networks in the human brain that show coherent patterns of activity. Similar intrinsic connectivity networks have been found in a variety of tasks, and various networks persist even during rest (Damoiseaux et al., 2006; Fox and Raichle, 2007; Smith et al., 2009). Such resting state networks are thought to arise due to the presence of predominantly low-frequency spontaneous variations in brain activity (Cordes et al., 2001; Fransson, 2005; Auer, 2008). The origin of these slow but coherent neural fluctuations is not well understood. Some

* Corresponding author. P.O. Box 30.001, 9700 RB Groningen, The Netherlands. Fax: +31 50 363 8875.
E-mail address: d.r.m.langers@med.umcg.nl (D.R.M. Langers).

1053-8119 © 2011 Elsevier Inc. Open access under the Elsevier OA license.
doi:10.1016/j.neuroimage.2011.01.019

networks are thought to be driven by internal mental processing, like the default mode network (Raichle and Snyder, 2007). Still, it seems reasonable to assume that sensory information contributes to drive such networks or to modulate their ongoing activity (Grossberg, 1999; Friston, 2009). With that in mind, intrusive ASN may well influence the activity of intrinsic brain networks during rest, even if these are not nominally associated with sound processing. Yet, despite its potentially widespread influence on spontaneous brain activity in fMRI, the presence of ASN has so far largely been neglected in the context of functional connectivity analyses.

At first glance, the same issues that play a role in conventional behavioral paradigms may also occur in resting state studies. Connectivity measures quantify the presence of coherent fluctuations in brain activity, whether evoked or spontaneous. If brain systems are driven into a state of constant activity by the presence of ongoing ASN, the acquired BOLD fMRI signals may conceivably saturate near a fixed ceiling (Langers et al., 2005b). This might result in less signal variation, rendering relationships regarding functional behavior more difficult to detect. However, contrariwise, ASN might also augment the magnitude of neural fluctuations when taking modulatory interactions into consideration. For instance, whereas the auditory cortex might show little activity in the absence of any acoustic stimulation, in the presence of ASN its activity could be high when the subject is attending to the acoustic environment but lower when the subject is focusing on other input (Woods et al., 2009). Thus, ASN might enlarge the range of occurring signal variations by acting as a source of stimulation that may subsequently be subjected to sensory gating (Campbell et al., 2007; Mayer et al., 2009). In conventional approaches that model stimulus-evoked activity only, these modulations would not be registered unless they correlate with the experimental protocol. However, connectivity measures are sensitive to all sources of coherent signal variations, and may benefit from their presence.

In contrast with the prevailing notion that ASN primarily reduces sound-related responses in auditory processing centers alone, we entertain the option that ASN alters both spontaneous and evoked fluctuations in activity in much more widespread brain networks than previously thought. Our working hypothesis is that ASN broadly influences the observable functional relationships between brain regions, and that functional connectivity levels may be either increased or decreased in the presence of ASN compared to those in a more silent environment.

So far, intrinsic connectivity networks in fMRI have almost exclusively been studied with noisy scanning methods. The current study was set up to investigate the effects of the accompanying ASN on the outcomes of various functional and effective connectivity measures in healthy subjects. In addition to conventional noisy acquisition schemes, sparse scanning methods were employed that are commonly used to mitigate the effects of ASN in dedicated study designs (Hall et al., 1999). We considered not only the central auditory system but also other intrinsic brain networks, both in task-related and resting state designs.

Materials and methods

Subjects

Twelve healthy subjects (7 M, 5 F; mean 25 y, range 21–35 y) were invited to participate in this fMRI study on the basis of written informed consent, in approved accordance with the requirements of the institution's medical ethical committee. All subjects were right handed (Oldfield, 1971). They reported no history of auditory, neurological, or psychiatric disorders. Standard clinical audiometry was performed to confirm that all subjects had normal hearing. Hearing thresholds amounted to 11 ± 6 dB HL (mean $\pm$ SD; averaged over all subjects, both ears, and frequencies of 250–8000 kHz). One subject was excluded after data preprocessing because of excessive head motion due to urinary urges during the imaging session.

Data acquisition

Subjects were placed supinely in the bore of a 3.0-T MR system (Philips Intera, Best, the Netherlands), which was equipped with a standard 8-channel phased-array (SENSE) transmit/receive head coil. The functional imaging session consisted of eight runs of almost 7 min duration, each consisting of a dynamic series of identical T_2*-sensitive whole-brain multislice gradient/field-echo echo-planar imaging (EPI) volume acquisitions (TE 23 ms; TA 2.0 s; FA 90°; matrix $64 \times 64 \times 48$; resolution $3.0 \times 3.0 \times 3.0$ mm^3; EPI factor 25; interleaved slice order, no slice gap). Initial preparation scans were used to achieve stable image contrast and to trigger the start of stimulus delivery, but these were not included in the analysis. Subjects wore ear plugs and a headset to dampen the ASN to approximately 70 dB SPL. The scanner coolant pump and fan were turned off during imaging to further diminish ambient noise levels.

The runs differed from each other with respect to the acquisition method, labeled *continuous* or *sparse*, and the behavioral paradigm, labeled *rest* or *task*. Together, this gave 4 possible combinations, for each of which two runs were performed (see Fig. 1). In the continuous runs, images were acquired without interruption (200 volumes; TR 2.0 s); in the sparse runs (Hall et al., 1999), functional acquisitions were alternated with 8.0-s periods of scanner inactivity (40 volumes; TR 10.0 s). In the rest runs, subjects were instructed to remain awake and lie still with their eyes open, but no task was imposed and no stimuli were delivered; in the task runs, subjects performed an auditory memory task that involved the presentation of sound stimuli through MR-compatible electrodynamic headphones (MR Confon GmbH, Magdeburg, Germany) (Baumgart et al., 1998).

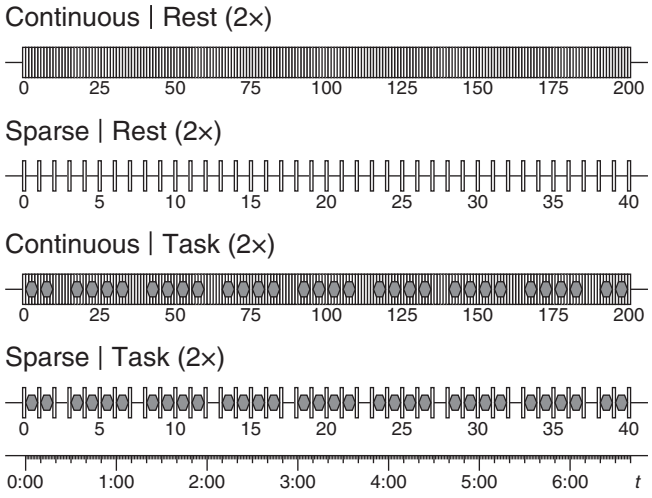

Fig. 1. Experimental design. Four different types of functional runs were acquired. Each 2-s EPI acquisition is illustrated in the form of a vertical open bar; each 8-s sound stimulus is represented as a shaded hexagon. Two acquisition methods (continuous and sparse) were combined with two task paradigms (rest and task). During continuous scanning, 200 image volumes were acquired without interruption. In contrast, the 40 sparse acquisitions were separated by periods of scanner inactivity. Additional preparation scans (labeled '0' in the figure) were executed but were not analyzed. The rest runs did not include any task performance or stimulus presentation. The task runs included the presentation of a series of diverse sound fragments, including one silent interval among every five consecutive fragments. Subjects were instructed to memorize the fragments, and their recollection was tested after the fMRI session. The sound stimuli were presented during the periods of scanner inactivity for the sparse runs, and at corresponding moments (while the scanner was active) for the continuous runs. Each type of run was repeated twice per subject, and corresponding runs were pair-wise concatenated for further analysis.

The memory task comprised a diverse series of 64 different 8.0-s sound fragments that were presented at intensity levels of approximately either 40 or 70 dB SPL. Stimuli included artificial waveforms and environmental noises of divergent spectrotemporal complexity, animal sounds, music, and vocalizations (http://audio-fmri.langers.nl/soundfiles.html). The sound fragments were timed such that they coincided with the silent intervals between consecutive scans in the sparse runs. The timing of the continuous runs was chosen in such a way that every fifth scan corresponded exactly with one of the sparse scans (i.e., continuous scans #5,10,15,…,200 corresponded with sparse scans #1,2,3,…,40). In other words, the periods during which sound fragments were presented were precisely filled with four acquisitions in the continuous runs. To limit the difficulty of the task, each fragment was presented twice: once during a continuous run, with interfering ASN, and once during a sparse run, on a silent background. In the middle of every block of five consecutive stimuli (i.e., directly preceding the sparse scans numbered #3,8,13,…,38), a fragment was inserted that contained silence only.

Prior to the fMRI session, the subjects were informed that their recollection of the sound stimuli would be tested afterwards. This test took place outside of the scanner environment, immediately after the fMRI session. All 64 familiar sound fragments were mixed with 64 novel sound fragments and presented in random order. For each subject, a different subset of 64 stimuli out of the complete set of 128 sound fragments was used in the fMRI session. Subjects reported whether they recognized the fragments from the fMRI session by means of a two-alternative forced choice questionnaire (i.e., by answering either 'yes' or 'no'). The main purpose of the behavioral task was to promote and monitor alertness of the subject during the MRI session.

Preprocessing and linear regression

During data processing, we used MatLab (The MathWorks Inc.), supplemented with a subset of processing routines from the SPM5 software package (Wellcome Department of Imaging Neuroscience, http://www.fil.ion.ucl.ac.uk/spm/) and the Group ICA of fMRI Toolbox v.1.3e (GIFT, http://icatb.sourceforge.net/groupica.htm).

Contrast differences between odd and even slices due to the interleaved slice order were eliminated by interpolating between pairs of adjacent slices, shifting the imaging grid over half the slice thickness. Next, the functional imaging volumes were corrected for motion effects using 3-D rigid body transformations. The anatomical images were coregistered to the functional volumes, and all images were normalized into MNI stereotaxic space using affine transformations. To improve signal-to-noise characteristics and to equalize the effective resolution within and across slices, but still retain sensitivity to activation in small sub-cortical processing nuclei (like the inferior colliculi), all images were moderately smoothed using an isotropic 5-mm full width at half maximum (FWHM) Gaussian kernel. A logarithmic transformation was carried out in order to naturally express all derived voxel signal measures in units of percentage signal change (given the small relative magnitude of the BOLD effect, a truncated Taylor series expansion of the transformed signal $\hat{S}(t) = 100 \cdot \ln(S(t))$ gives rise to $\Delta\hat{S}(t) = 100 \cdot \Delta S(t)/S_0$, indicating that the absolute signal change in $\Delta\hat{S}(t)$ equals the relative signal change in $\Delta S(t)$ expressed as a percentage relative to its baseline level S_0).

Mass-univariate general linear regression models (GLMs) were constructed and assessed for each subject, including: [i] boxcar functions, modeling the sound presentations; [ii] 3rd-degree polynomials for each run, modeling baseline and drift effects; [iii] translation and rotation parameters in the *x*-, *y*- and *z*-direction, modeling residual motion; and [iv] the average signal of all brain voxels, modeling global mean signal variations. The estimated sound-evoked response amplitudes were entered into a group-level random effects analysis. The other regressors (ii–iv) were considered confounds, and their estimated effects were subtracted from the preprocessed functional imaging volumes prior to the functional connectivity analyses that followed.

Independent component analysis

Within each subject, the pairs of runs of identical type were concatenated, resulting in two 80-volume sparse runs (one rest and one task) and two 400-volume continuous runs (idem). The dimensionality of the available data was reduced in three stages by retaining only the strongest principal components (Calhoun et al., 2001). First, the four types of runs were each reduced to an equal number of 24 components. Next, an aggregate dataset was constructed by concatenating these four reduced runs in time, and reducing the result again to 24 components. Finally, the data of all subjects were similarly concatenated and reduced back to 24 components. This last step was applied to the aggregate data, but in parallel also to the reduced data of each of the four types of runs separately.

Multivariate spatial independent component analysis (ICA) was performed using the InfoMax algorithm to extract maximally independent components (Bell and Sejnowski, 1995). The concatenated component time courses were scaled to unit variance; the corresponding spatial maps were scaled in the opposite direction such that their outer product remained the same. As a result, the spatial maps contained the spatial distribution of the root-mean-square component amplitude (expressed in percentage signal change units), while the time courses described the components' signal dynamics only (in dimensionless units). In the end, five sets of 24 group-level independent components were obtained: one set for the aggregate data that contained all four types of runs in equal proportion, and four more sets for each of the types of runs separately.

Because independent components have no meaningful order by themselves, the five sets were retrospectively brought into correspondence by matching the component maps from the aggregate set one-on-one to those from each of the four other sets. This was achieved in an automated manner using the Kuhn-Munkres algorithm by maximizing a combined similarity measure that is based on the pair-wise inner products between component maps (Langers, 2010).

Six components were subjectively interpreted to arise from MR-imaging artifacts, for instance related to interactions between pulsatile motion, spin-history, relaxation, and magnetic susceptibility. These were largely confined to the 'edges' of the brain (in particular on the ventral side and surrounding the brainstem), were spread out widely but sparsely, or tended to co-localize with CSF compartments. The other eighteen components were deemed to be of neural origin on the basis of their coherent spatial distribution that well corresponded with particular gray matter brain structures (Smith et al., 2009; Schöpf et al., 2010). Ten components were selected for detailed analysis, either because their time courses and corresponding spectra suggested the presence of evoked responses in relation to the employed stimuli and task in the task runs, or because they contained brain systems that were otherwise considered to be of potential interest. The rejected neural components typically comprised brain systems that already appeared to be represented in some of the selected components, that were considered unrelated to the task, or that were judged to be insufficiently well separated from artifactual signal contributions.

The time courses of the selected aggregate independent components were partitioned according to subject, and according to the four types of runs. The resulting single-run data were Fourier transformed to obtain logarithmic power spectra. To eliminate differences due to spectral aliasing and to minimize confounding effects of hemodynamic delays, the outcomes for the continuous runs were sub-sampled to the same temporal resolution as the sparse runs by retaining acquisitions #5,10,…,400 only. No averaging or temporal filtering was carried out before this decimation process. Subsequently, component data were fitted by means of linear regression: time courses were fitted with a constant

offset to model the silent baseline as well as a boxcar function representing the sound presentations (equal to 0.0 for volumes #3,8, …,78, and 1.0 otherwise); power spectra were fitted with a model that included an offset, a linear slope, and a single covariate to model peaks at 16 and 32 cycles/run (corresponding with the fundamental frequency of the silent fragments in the stimulus presentations, and its second harmonic). Only the data in the range of 8–39 cycles/run (i.e.: 0.01–0.05 Hz) were included in the spectral fit: lower frequencies were discarded because they were affected by the polynomial baseline and drift removal during preprocessing; higher frequencies exceeded the Nyquist frequency. Even though no stimuli were presented in the rest paradigm, the same models were used for all runs (including the evoked response terms) to allow paired comparisons to be made on the estimated coefficients.

Connectivity analysis

Eighteen ROIs were placed near local maxima of the major active regions in the maps of the ten selected independent components of interest. All ROIs were equal in size and consisted of two small clusters of 19 voxels each (one central voxel, plus its six face- and twelve edge-neighbors). These were mostly positioned symmetrically in left and right homologous areas of the brain. Exceptions were made for activated areas that were confined to the vicinity of the midsagittal plane, for which the two clusters were both centered on this plane. Also, for areas that showed up only unilaterally in a particular component, both clusters were positioned in the same hemisphere; however, in these cases exact 'mirror-image' ROIs could always be defined on the basis of areas that showed up in another component. Fig. 7a illustrates the location of these ROIs. Table 1 provides a detailed list that includes MNI coordinates and nearest designations according to the Talairach Daemon anatomical labeling of the WFU PickAtlas toolbox (Lancaster et al., 2000; Maldjian et al., 2003); the corresponding lateralization is indicated in square brackets (L/M/R = Left/Midplane/Right).

Functional and effective connectivity analyses were performed. For all ROIs, time courses were determined for each of the four types of runs, averaged over all voxels in the ROI and concatenated across subjects. Functional connectivity maps were derived by calculating the Pearson correlation coefficients R between the ROI time courses and the time courses of all other voxels in the brain. Furthermore, 18×18 matrices $\boldsymbol{\Sigma}$ were determined that contained the covariances between all pairs of ROIs. A non-causal effective connectivity model was assessed by computing the concentration matrix $\mathbf{C} = \boldsymbol{\Sigma}^{-1}$, and deriving a matrix $\boldsymbol{\rho}$ containing partial correlation coefficients according to $\rho_{mn} = -C_{mn}/\sqrt{(C_{mm} \cdot C_{nn})}$ (Marrelec et al., 2006).

For a subset of pairs of ROIs (AUD–STS, CEN–MED, INS–ACC, PAR–PAL, MFG–PRE, and PCC–ANG), the partial correlation ρ_{mn} was

Table 1
Regions of interest (ROIs).

ROI	Description	Coordinates	Anatomical labeling
AUD	Auditory cortex	(−54,−15,+06) (+54,−15,+06)	Superior temporal gyrus [L] Superior temporal gyrus [R]
SMG	Supramarginal gyrus	(−60,−39,+30) (+60,−39,+30)	Inferior parietal lobule [L] Inferior parietal lobule [R]
PRE	Precuneus	(−06,−57,+48) (+06,−57,+48)	Precuneus [L] Precuneus [R]
MFG	Middle frontal gyrus	(−30,+30,+42) (+30,+30,+42)	Middle frontal gyrus [L] Middle frontal gyrus [R]
THA	Thalamus	(−12,−06,+15) (+12,−06,+15)	Extra-nuclear [L] Extra-nuclear [R]
STS	Superior temporal sulcus	(−60,−33,−03) (+60,−33,−03)	Middle temporal gyrus [L] Middle temporal gyrus [R]
OFC	Orbitofrontal cortex	(−45,+18,+21) (+45,+18,+21)	Sub-gyral [L] Sub-gyral [R]
PAL	Left parietal cortex	(−39,−57,+42) (−30,−72,+42)	Inferior parietal lobule [L] Precuneus [L]
FRL	Left frontal cortex	(−30,+12,+54) (−45,+03,+45)	Superior frontal gyrus [L] Middle frontal gyrus [L]
PAR	Right parietal cortex	(+39,−57,+42) (+30,−72,+42)	Inferior parietal lobule [R] Precuneus [R]
FRR	Right frontal cortex	(+30,+12,+54) (+45,+03,+45)	Superior frontal gyrus [R] Middle frontal gyrus [R]
ACC	Anterior cingulate cortex	(±00,+33,+18) (±00,+18,+36)	Anterior cingulate [M] Cingulate gyrus [M]
INS	Insula	(−45,+15,−06) (+45,+15,−06)	Inferior frontal gyrus [L] Inferior frontal gyrus [R]
ANG	Angular gyrus	(−45,−69,+24) (+45,−69,+24)	Middle temporal gyrus [L] Middle temporal gyrus [R]
PCC	Posterior cingulate cortex	(−12,−54,+06) (+12,−54,+06)	Posterior cingulate [L] Posterior cingulate [R]
MED	Medial sensorimotor cortex	(±00,−15,+54) (±00,−33,+60)	Medial frontal gyrus [M] Paracentral lobule [M]
CEN	Pericentral sensorimotor cortex	(−42,−27,+57) (+42,−27,+57)	Postcentral gyrus [L] Postcentral gyrus [R]
VIS	Visual cortex	(−15,−81,−12) (+15,−81,−12)	Lingual gyrus [L] Lingual gyrus [R]

decomposed into frequency contributions as follows. Let the vectors $\mathbf{x}_m$ and $\mathbf{x}_n$ represent the centered partial signals of ROIs m and n (i.e., the signals of the two ROIs that remain after the signal mean as well as effects that are attributable to all other 16 ROIs have been removed by means of linear regression). Then, the partial correlation coefficient satisfies $\rho_{mn} = (\mathbf{x}_m/|\mathbf{x}_m|)^{\mathrm{T}}(\mathbf{x}_n/|\mathbf{x}_n|)$. Denote the discrete Fourier transforms of the signals $\mathbf{x}_m$ and $\mathbf{x}_n$ by $\boldsymbol{\xi}_m$ and $\boldsymbol{\xi}_n$. From Parseval's theorem, it follows that $\rho_{mn} = (\boldsymbol{\xi}_m/|\boldsymbol{\xi}_m|)^{\mathrm{T}}(\boldsymbol{\xi}_n/|\boldsymbol{\xi}_n|)$. In other words, the partial correlation coefficient can equally be expressed as a sum of terms in the temporal or frequency domain. Although the Fourier terms are complex-valued, the contributions from aliased frequencies form complex conjugate pairs and can be additively combined. Thus, the partial correlation can be spectrally decomposed into frequency terms that add to ρ_{mn}.

Statistical analysis

Group-level activation in the GLM was assessed by means of *t*-tests. Corrections for multiple comparisons to account for the multitude of voxels were based on Gaussian random field theory (Friston et al., 2007).

The regression coefficients that were derived from the independent component time courses were determined subject by subject, and submitted to single sample *t*-tests. Paired comparisons between outcomes of task and rest runs, as well as continuous and sparse runs, were made by performing *t*-tests on the differences. Interactions between the effects of the behavioral paradigm and acquisition method were assessed on the basis of a contrast vector of the form $[+1,-1,-1,+1]$.

The group-level significance of the obtained effective connectivity levels was evaluated by means of a bootstrap resampling method. Concatenated time courses were repeatedly constructed by randomly sampling – with replacement – eleven subjects from the available group, and partial correlation coefficients were determined on the basis of the resampled data. Ten million such outcomes were used to construct probability distributions for the effective connectivity levels of all connections between ROIs, and these were used to assess the significance of deviations from zero. A Bonferroni correction was applied for the 153 connections in the model.

Results

Task performance

The behavioral outcomes of the stimulus recollection test that was administered after the MRI session are summarized in Table 2. Of the 128 sound fragments that were presented during the test, 64 had already been presented during the fMRI paradigm, and 64 were new. For each fragment, subjects indicated whether they did or did not recognize the stimulus from the MRI session. The table includes the mean ± SE across subjects of the relative number of true positives (TP) that were correctly remembered, false positives (FP) that were mistakenly recognized, false negatives (FN) that were mistakenly not recognized, and true negatives (TN) that were correctly not remembered, each expressed as a percentage of the total number of fragments. Some incorrect answers (FP and FN) were given, but correct answers (TP and TN) were substantially more abundant and well above chance level. This suggests that the task was doable but not trivial. The derived sensitivity (SEN = TP/(TP + FN)), specificity (SPE = TN/(TN + FP)), positive predictive value (PPV = TP/(TP + FP)), and negative predictive value (NPV = TN/(TN + FN)) confirmed this impression.

Table 2
Behavioral outcomes.

Measure	Outcome
TP	37 ± 2%
FP	10 ± 2%
FN	13 ± 2%
TN	40 ± 2%
SEN	73 ± 4%
SPE	80 ± 3%
PPV	79 ± 2%
NPV	76 ± 2%
$SEN_{40,continuous}$	67 ± 4%
$SEN_{70,continuous}$	64 ± 5%
$SEN_{40,sparse}$	79 ± 4%
$SEN_{70,sparse}$	81 ± 4%

The sensitivities to stimuli of 40 or 70 dB SPL in the presence or absence of ASN (continuous or sparse, respectively) are listed separately. According to paired *t*-tests, the stimuli from the sparse runs were remembered significantly better on average than those from the continuous runs, both for the 40-dB ($p = 0.001$) and the 70-dB ($p = 0.0004$) presentation levels, but the louder stimuli were not remembered differently from the softer stimuli ($p > 0.1$). However, note that because all presented stimuli were played twice during different runs, these figures may be distorted and differences between the various types of runs diminished (for example, a 40-dB sound fragment that was presented during a continuous run may have been completely inaudible, but still recognized correctly if it was also presented at 70 dB during a sparse run). As a result, performance for the stimuli during the continuous runs alone might have been close to the 50% chance level, and for the sparse runs alone above 90%. But the finding that stimuli were remembered best in the absence of ASN remains.

General linear model (GLM)

Conventional regression analysis was applied to the task runs by means of a mass-univariate random effects model (Friston et al., 2007). Fig. 2 displays the significance of sound-evoked brain activity at the group level, as obtained by contrasting the mean fMRI signal following sound presentations with baseline. Although for both the continuous and the sparse runs extensive activation was observed in the bilateral superior temporal lobes containing auditory cortex, activation was most significant and extensive in the sparse runs. Furthermore, task-related activity was observed in the lateral frontal lobe, again most strongly in the sparse runs. Finally, in the sparse runs, the analysis revealed activation in various sub-cortical auditory nuclei (like the inferior colliculi) and in the cerebellum, as well as deactivation in various regions associated with the default mode network (medial and lateral areas in the parietal and frontal lobes). These areas did not achieve significance in the continuous runs.

Independent component analysis (ICA)

The spatial maps of ten extracted neural components of interest are shown in Fig. 3. On the basis of the included brain areas these were labeled as: [I] auditory cortex; [II] precuneus and supramarginal gyrus; [III] thalamus and putamen; [IV] auditory association cortex; [V] left frontal and parietal cortex; [VI] right frontal and parietal cortex; [VII] anterior cingulate cortex and insula; [VIII] posterior cingulate and medial prefrontal cortex; [IX] sensorimotor cortex; and, [X] visual cortex. The maps of corresponding components were remarkably comparable across all types of runs (whether resting state or task-related, continuous or sparse), despite the fact that they were separately derived from independent datasets. In Fig. 5a, each component's overall root-mean-square (RMS) amplitude A is plotted.

In the components I–III, the spatial maps depended strongly on the type of run. In the auditory cortex (I), signals were much stronger during the task runs than during the rest runs. A weaker but significant dependence upon the acquisition method was found: in the rest runs, signals were marginally stronger during continuous

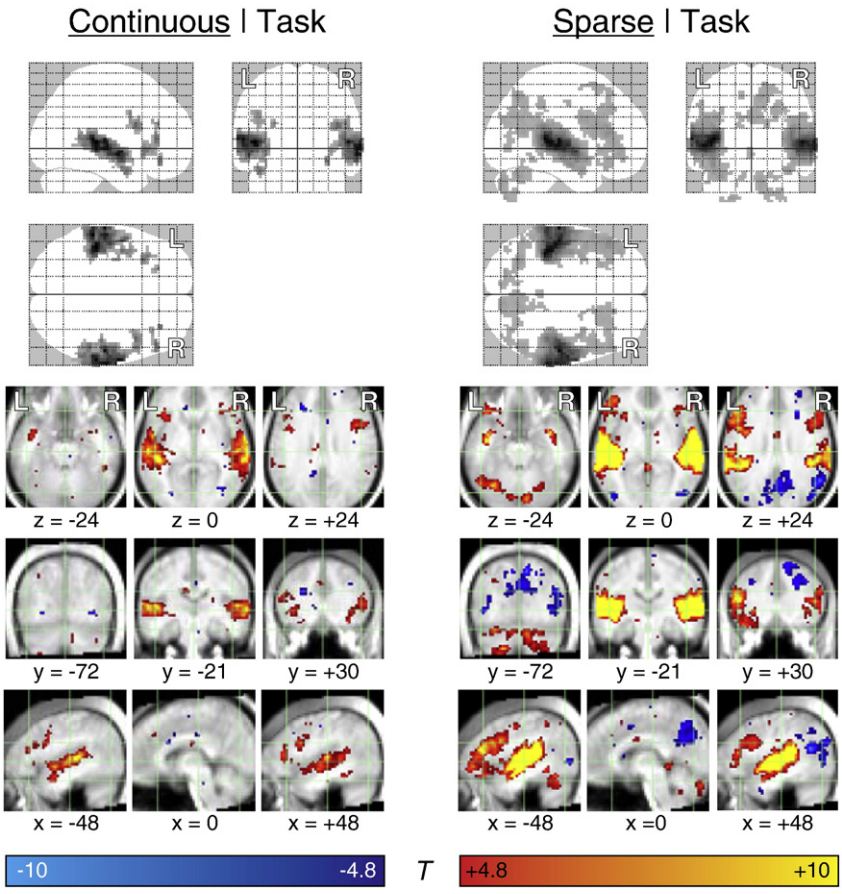

Fig. 2. Sound-evoked activation. Group-level evoked activation was determined by means of a conventional linear regression model for the continuous (left) and sparse (right) task runs separately. The glass brain views (top) show the outcomes of voxel-wise two-tailed *t*-tests by means of grayscale coloring. In addition, various axial, coronal, and sagittal cross-sectional images (bottom) display positive as well as negative activation by means of a color code; in each image, the maximum activation in 5 contiguous slices was projected on an anatomical background. All images were thresholded at a confidence level $p<0.05$, corrected for family-wise errors (FWE); for the glass brain, a minimum cluster size of $k=10$ voxels was additionally imposed. Sound-evoked activation was primarily found in the temporal and frontal lobes, most extensively and confidently in the runs with sparse acquisitions as compared to the continuous ones. Stimulus-related activation in sub-cortical auditory nuclei and in the cerebellum as well as deactivation in the default mode network was observed in the sparse runs only.

runs, while in the task runs, signals were strongest during sparse runs. The interaction between behavioral paradigm and acquisition method was significant. In the second component (II), the precuneus as well as bilateral frontal areas were most extensively represented in the two rest runs. In addition, weaker clusters were found near the supramarginal gyrus. For the component that comprised superior thalamic regions and the putamen (III), the level and extent of activity was dependent upon task performance, but did not depend upon the acquisition method.

In the components IV–VII, little dependence upon the type of run was visible in the maps, although overall component power was significantly different in some paired comparisons. The auditory association cortex (IV) was similarly active in all runs, except the sparse task run. This component also included ventrolateral frontal regions. Next, two components were found that appeared to be each other's mirror images. Although homologous bilateral areas in frontal and parietal cortex were involved, they were strongly lateralized towards the left (V) and right (VI) hemisphere, respectively. Finally, the insula and anterior cingulate gyrus were grouped in one component (VII). This also included activation of medial prefrontal cortex, with varying sign.

The components VIII–X showed little dependence upon the type of run in the maps, and none of the comparisons of component power reached significance. One component (VIII) comprised bilateral active clusters near the junction of the angular gyrus and middle occipital gyrus, a more medial cluster near the junction of the posterior cingulate gyrus and the ventral part of the precuneus, and a cluster in the medial prefrontal cortex. Although this is reminiscent of the default mode network in component II, this component did not appear to differ between task and rest. Another component (IX) contained the somatosensory and motor cortex in lateral and medial areas surrounding the central sulcus. In spite of the absence of any motor task, it appeared marginally stronger in the task runs. However, the difference was insignificant. Finally, activity of the visual cortex in the inferior posterior occipital lobe (X) did not appear to depend on the type of run at all.

The time courses and corresponding power spectra of the ten components are graphed in Fig. 4. These data were fitted with regression

Fig. 3. Independent component maps. The spatial distribution of the extracted independent components was determined from the component's root-mean-square signal amplitude in all voxels (*A*, expressed in percentage signal change units [%]). The maps of ten selected components of interest (I–X) are superimposed on an anatomical background. In all cross-sectional images, the activity in 5 adjacent slices was overlaid by means of a color code using a maximum intensity projection. In each panel, three perpendicular views on the left provide an overview of the component. These maps were derived from the aggregate data, including continuously as well as sparsely acquired volumes, both during rest as well as task paradigms. Immediately on their right, corresponding axial cross-sections are shown of the components that were extracted from the various types of runs separately. These involved either continuous (left column) or sparse (right column) acquisitions, and either rest (top row) or task (bottom row) paradigms. Each component was present in comparable fashion for most types of runs. Nevertheless, the type of run affected the distribution and strength of various components, in particular for components I, II, and III.

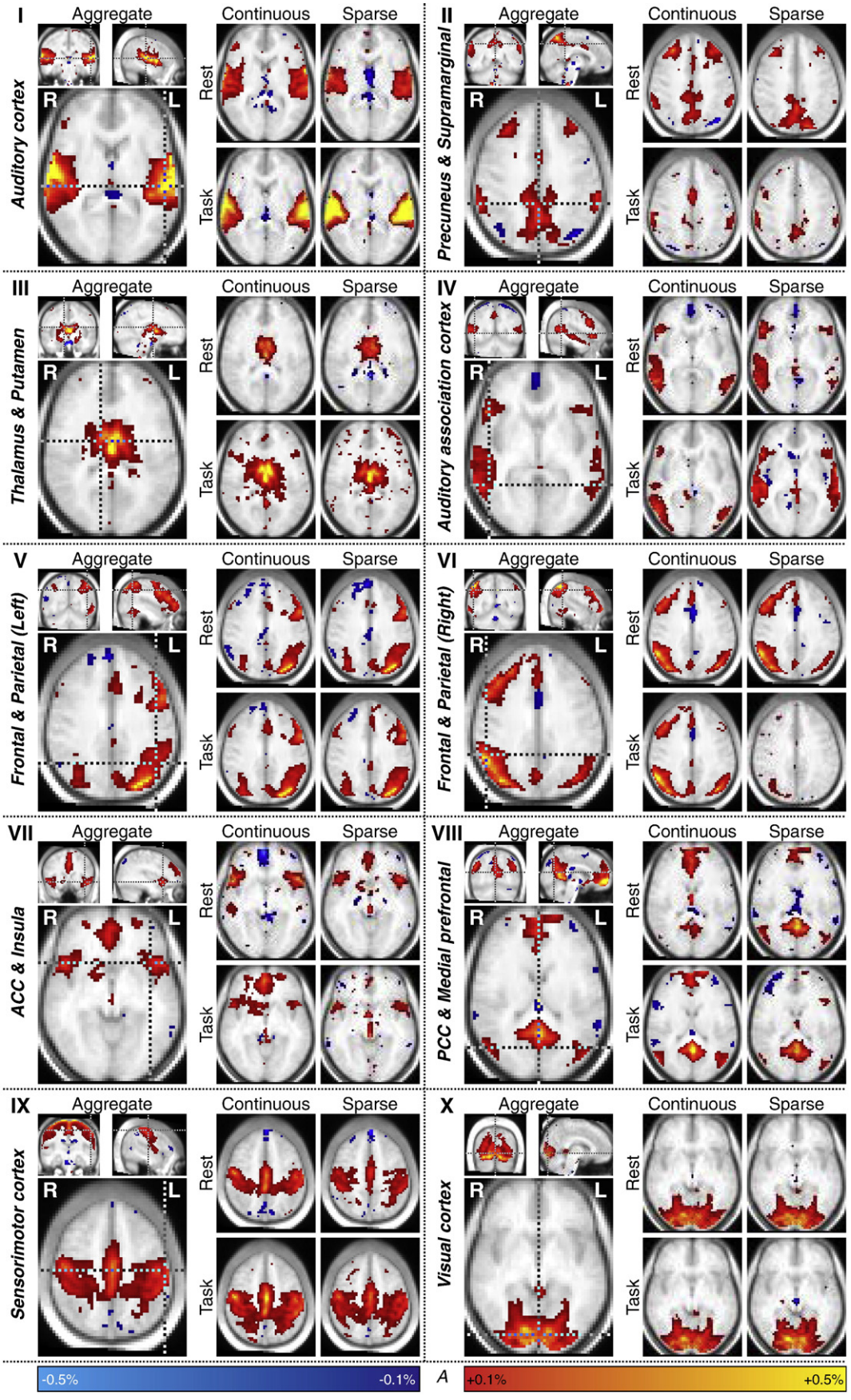
I
Auditory cortex
II
Precuneus & Supramarginal
III
Thalamus & Putamen
IV
Auditory association cortex
V
Frontal & Parietal (Left)
VI
Frontal & Parietal (Right)
VII
ACC & Insula
VIII
PCC & Medial prefrontal
IX
Sensorimotor cortex
X
Visual cortex
Aggregate
Continuous
Sparse
Rest
Task
R
L
-0.5%
-0.1%
A
+0.1%
+0.5%

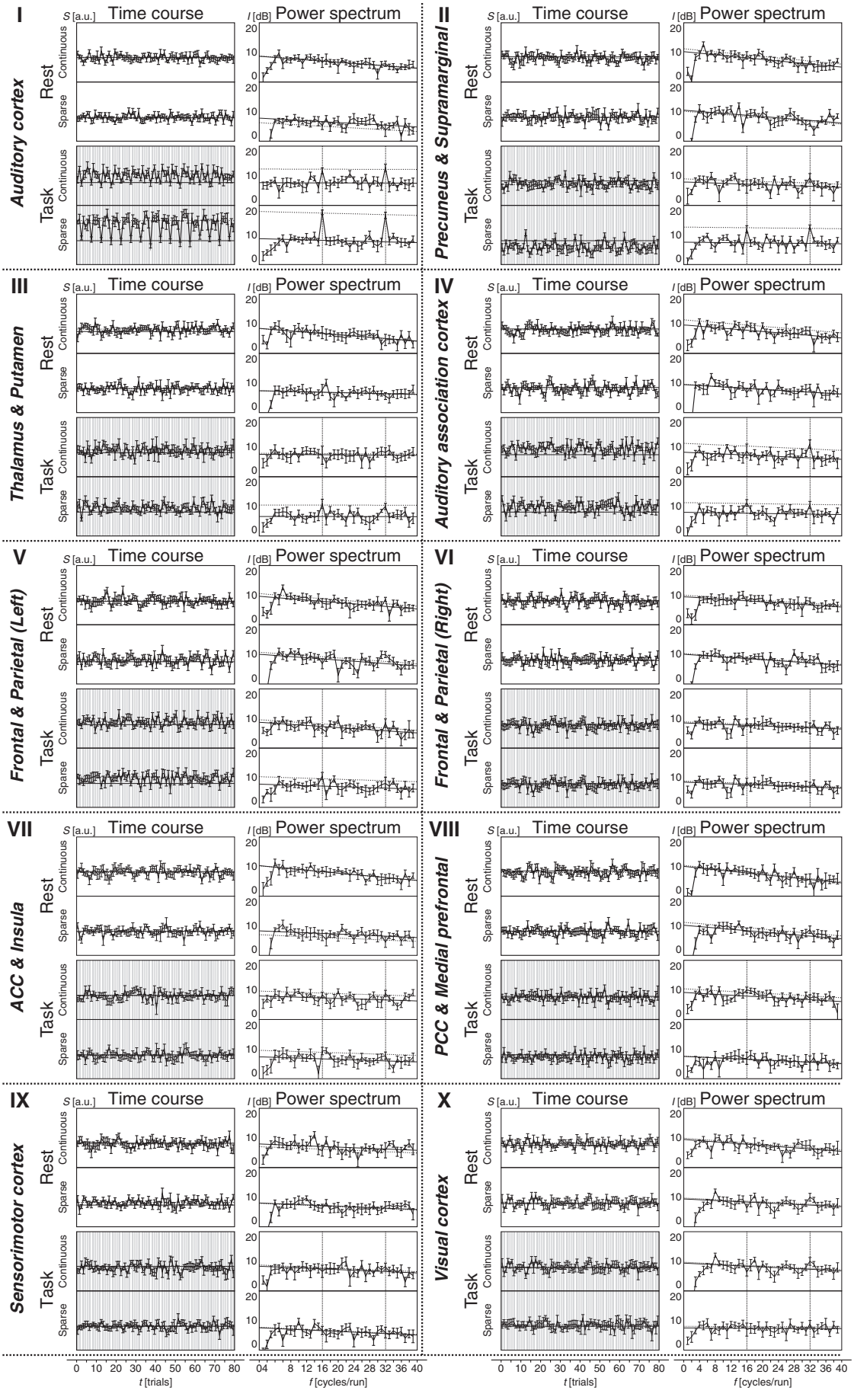
I
Auditory cortex
II
Precuneus & Supramarginal
III
Thalamus & Putamen
IV
Auditory association cortex
V
Frontal & Parietal (Left)
VI
Frontal & Parietal (Right)
VII
ACC & Insula
VIII
PCC & Medial prefrontal
IX
Sensorimotor cortex
X
Visual cortex
Time course
Power spectrum
S [a.u.]
I [dB]
Rest
Task
Continuous
Sparse
t [trials]
f [cycles/run]

models, and the resulting coefficients and significance levels are summarized in Figs. 5 b–d. In addition, the mean spectra of all ten reported components are overlaid in Fig. 6, providing a more direct summary comparison of the four different types of runs.

For the rest runs, all time courses were essentially random due to the lack of a shared source of activation. A deficit in spectral power existed at frequencies below ~4 cycles/run (~0.005 Hz). This was attributed to low-frequency drift removal during preprocessing, and was therefore not judged meaningful (Smith et al., 1999). A more gradual decline towards higher frequencies was observed. Almost invariably, the magnitude of the decline was strongest and most significant for the rest runs (see Figs. 5d and 6). The slope in the sparse runs was typically less pronounced than in the continuous runs, but still stronger than in both types of task runs.

In the task runs, several components showed pronounced sound-evoked responses. These were visible in the form of distinct periodic signal drops in the time courses whenever sound stimuli were absent (at trials #3,8,13,…,78; see also Fig. 5b), and corresponding peaks in the spectra (at 16 and 32 cycles/run; see also Fig. 5c). This type of behavior was most prominent in the auditory cortex (I), but also significant in the thalamus and putamen (III), auditory association cortex (IV), and to a lesser extent the frontoparietal cortex (V and VI). In the component that comprised the precuneus and supramarginal gyrus (II), evoked responses were strong as well, but with opposite sign. Sound-evoked effects were typically smaller and less significant during continuous acquisitions than during sparse acquisitions. Regarding the mentioned components, interaction effects between acquisition method and behavioral paradigm were significant in the auditory cortex (I) and precuneus and supramarginal gyrus (II).

Effective connectivity analysis (ECA)

In an effort to gain insight into interactions between the involved brain areas and distinguish between direct and indirect functional connections, an effective connectivity analysis based on partial correlation coefficients (Marrelec et al., 2006) was carried out. Eighteen ROIs were defined that appeared prominently in the various independent components (Table 1). In Fig. 7b, for each of the four types of runs, ROIs for which the effective connectivity level was significantly larger than zero are connected by means of a solid line.

Auditory cortex (AUD) connected to the superior temporal sulcus (STS) in the task runs, but not in the rest runs. The precuneus (PRE) and middle frontal gyrus (MFG) were always connected, in accordance with the fact that they were grouped into the same independent component. Similarly, insula (INS) and anterior cingulate cortex (ACC) were always connected. INS connected to STS and supramarginal gyrus (SMG) in all runs except the sparse task one. The left and right parietal and frontal areas (PAL, FRL, PAR, and FRR) showed a very strong 'horseshoe-shaped' connectivity pattern of the form FRL-PAL-PAR-FRR; no direct interhemispheric connections between the frontal areas were revealed, except for a relatively weak connection in the continuous rest run. The effective connectivity level between posterior cingulate cortex (PCC) and angular gyrus (ANG) was significant in all runs except the sparse task one. The medial (MED) and pericentral (CEN) sensorimotor areas connected very strongly in all types of runs. The orbitofrontal cortex (OFC) connected inconsistently to few other areas. The visual system in the inferior occipital lobe (VIS) and superior thalamus (THA) typically occurred in strict isolation.

For six pairs of ROIs, Fig. 7c plots the cumulative partial correlation as a function of frequency. For the connections AUD-STS and CEN-MED, the achieved effective connectivity levels in the task runs diverged substantially from those in the rest runs. For the connection between AUD and STS, this was primarily driven by the periodicity of the task paradigm (most notably present as a 'staircase' behavior in the sparse runs). For the connection between CEN and MED, correlations diverged most notably at high frequencies (15 cycles/run and above). For all other runs, differences between the four types of runs were small in comparison, unsystematic, and judged insignificant. For PAR-PAL, correlations remained comparable up to 30 cycles/run, and subsequently diverged weakly. For the connections INS-ACC and PCC-ANG, cumulative correlations remained closely clustered, although the continuous task runs resulted in higher partial correlations; in contrast, for the connection MFG-PRE the sparse task run deviated upward from the other three.

For each of the ROIs we also constructed functional connectivity maps, containing Pearson correlation coefficients between the ROI time course and the time courses of each of the individual voxels in the brain. These are included in the Supplementary Materials. Most notably, the functional connectivity within the auditory cortices was higher in the task runs than in the rest runs on the basis of the AUD maps. A similar but weaker trend was visible in the maps derived from STS and OFC, and to a lesser degree in PRE, MFG, ACC, MED and CEN. The acquisition method had hardly any influence on the functional connectivity results for any of the ROIs, including AUD. In other words, sparse and continuous acquisitions always resulted in indistinguishable functional connectivity outcomes.

Comparison of GLM, ICA, and ECA outcomes

Regardless that the GLM, ICA, and ECA methods extract functional measures with completely different interpretations, we made a comparison of the effects of ASN on their primary outcomes. For the GLM, the percentage signal change β in the significantly activated voxels was considered (see Fig. 2). For the ICA, the RMS amplitude A in the set of voxels that exceeded the imposed threshold in the aggregate data was included (see Fig. 3). For the ECA, the effective connectivity level ρ between all pairs of ROIs was taken, regardless of significance (see Fig. 7). The results from the sparse runs in the absence of ASN are plotted as a function of the equivalent results from the continuous runs in the presence of ASN in Fig. 8.

For both the GLM and ECA analyses, results correlated strongly ($R=+0.89$ and $R=+0.83$, respectively). The correlation of the ICA results was lower ($R=+0.59$), partly due to the fact that all ten components were included these data (including some components that were significantly affected by ASN, like the auditory component, and other components that were not). More relevant than the correlation coefficients, the ratios between results from runs with and without interference from ASN were determined on the basis of the principal component axes of these data. Whereas the presence of ASN diminished the magnitude of detectable sound-evoked responses by a factor of 2.27 in the GLM, the outcomes of the ICA were less affected and differed by a factor of 1.21 only. The ECA connectivity levels diverged less still, and differed merely by a factor of 1.07.

Fig. 4. Independent component time courses and power spectra. The time courses of ten neural independent components from the aggregate data (I–X; see also Fig. 3) were partitioned according to the four different types of runs (continuous or sparse acquisitions, and rest or task paradigms). In each panel, the extracted time courses are shown on the left (S, in arbitrary units [a.u.]), and the corresponding power spectra on the right (I, in decibel [dB] relative to an arbitrary reference). Error bars indicate the mean and standard error across subjects. For the task runs, the timing of the sound presentations is indicated by means of background shading in the time courses. The repetition rate of the corresponding periodicity (i.e.: one silent period in every five fragments) and its second harmonic are indicated by means of vertical dotted lines in the spectra. Straight lines show the outcomes of linear fits to baseline (solid) and evoked (dashed) activity. Even though the rest runs did not include sound presentations, the same regression models (including evoked response terms) were used for all runs. Fitted coefficients are reported in Fig. 5.

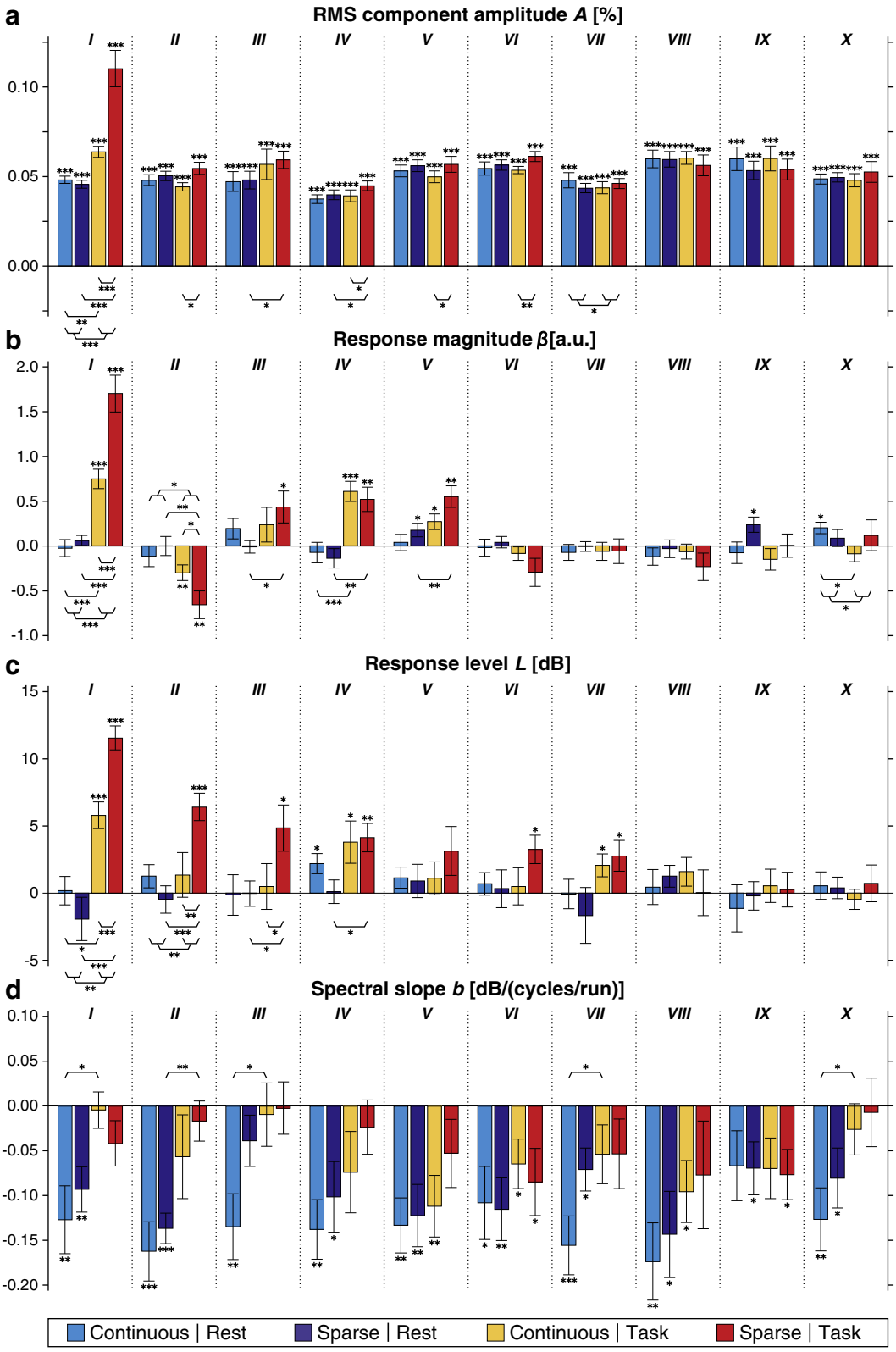

Fig. 5. Four measures of independent component dynamics across subjects and paradigms. The time courses and spectra of ten independent components were determined (see Fig. 4), and fitted by means of linear regression. [a] The total root-mean-square (RMS) component amplitude (A, expressed in percent signal change [%]) was determined as the product of the total RMS signal amplitude in the component maps and time courses. [b] The response magnitude (β, expressed in dimensionless arbitrary units [a.u.]) indicates the amplitude of the boxcar-shaped response in the time domain, i.e. the conventional fMRI contrast sound vs. silence. [c] The response level (L, expressed in decibel [dB]) equals the average magnitude of the two stimulus-evoked peaks at 16 and 32 cycles/run relative to the background spectrum. [d] The spectral slope (b, expressed in [dB/(cycles/run)]) represents the 1st-order coefficient of a linear fit through the spectrum, excluding the task-induced peaks and the initial upward slope at low frequencies. Parameters are reported for rest and task, continuous and sparse runs, separately. The group-level significance of deviations from zero on the basis of Student t-test statistics are indicated (*: $p<0.05$; **: $p<0.01$; ***: $p<0.001$; uncorrected). In addition, brackets report the significance according to paired t-tests for the differences between continuous and sparse acquisitions, differences between rest and task paradigms, and interactions between acquisition method and paradigm.

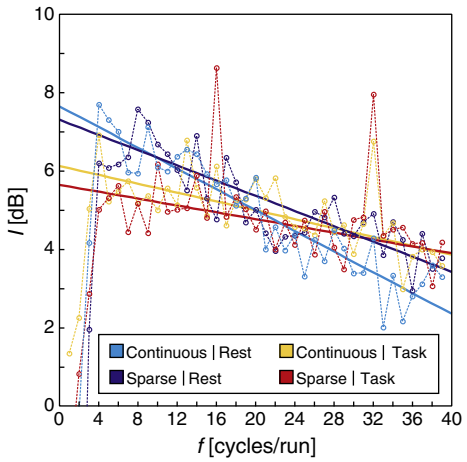

Fig. 6. Average component spectra for four types of runs. The independent components' spectra were determined and averaged over ten selected components of interest (see Fig. 4). The results for the four different types of runs are overlaid in a single figure, together with a linear fit to the data in a frequency range of 8–39 cycles/run (the spectral fall-off below 4 cycles/run is attributable to data preprocessing, in particular scanner drift removal). The spectra of both types of resting state runs were dominated by low-frequency oscillations, whereas those from the task-related runs were significantly flatter. Within the resting state runs, the runs with continuous acquisitions and ongoing scanner noise showed a noticeably steeper profile than those with sparse acquisitions and interleaved scanner noise.

Discussion

The advantages of sparse imaging over continuous acquisitions in the context of an auditory task are demonstrated by the outcomes of our conventional linear regression analyses. Extensive sound-evoked or task-related activation was detected by the GLM. The activity in bilateral primary and secondary auditory cortex and auditory association cortex reflects sensory processing related to sound perception. The observed frontal activation reflects cognitive processes related to executive control in relation to the memory task. In agreement with previous findings (Gaab et al., 2007; Scarff et al., 2004; Langers et al., 2005b; Tomasi et al., 2005), the interference from ASN during the continuous runs resulted in a substantial decrease of the detectable activation level and extent in all of these areas. Moreover, various task clusters were revealed in the sparse runs that could not be detected at all in the continuous runs. These comprised activation in sub-cortical auditory nuclei (Langers et al., 2005a), as well as deactivation in the default mode network (Gaab et al., 2008). Clearly, in experiments that aim to detect neural activation during acoustic tasks, sparse sampling provides the largest response amplitude, the highest sensitivity, and the best discriminatory power.

We attribute the observed differences in activation between continuous and sparse runs to interference from the MR-scanner. At least three mechanisms can be distinguished that may have caused the detected brain regions to respond differently. First, interactions occurred at the perceptual level, in the form of a direct masking of presented auditory stimuli by simultaneous ASN. This is supported by the fact that subjects performed significantly worse in memorizing sound fragments in the presence of ASN. Second, even when auditory stimuli and ASN do not coincide exactly, brain responses that are evoked by the perception of ASN may elevate baseline activity as detected by fMRI. Given the limited dynamic range of hemodynamic responses in the capillary bed, saturation will occur, and detectable responses to additional presented stimuli can be reduced. Third, the gradient switches or radio-frequency excitations that are associated with the acquisition of functional MRI volumes have been reported to influence brain function directly (Robertson et al., 2010; Rohan et al., 2004). The interaction between strong electromagnetic fields and brain activity is the basis for transcranial magnetic stimulation (TMS), a potential therapeutic means to alleviate various neural disorders, including some related to sound processing, like auditory hallucinations and tinnitus (López-Ibor et al., 2008). However, for the particular EPI acquisitions that are commonly employed in fMRI, evidence for direct electromagnetic effects is weak. We therefore suspect that electromagnetic effects are negligible in comparison with the aforementioned perceptual and hemodynamic interactions.

ICA succeeded in reliably extracting a multitude of components that corresponded with brain systems of interest. Components with a highly similar spatial distribution were identified across all types of runs, in spite of the notable differences in paradigm (an auditory memory task vs. resting state) and acquisition method (sparse vs. continuous scanning). A comprehensive 'task-positive' network was observed, consisting of at least the components I, III, and IV. In addition, a 'task-negative' network was detected, consisting of component II. Their putative involvement will be discussed in more detail.

Component I comprised primary and secondary areas of auditory cortex. These are the targets of the classical auditory pathway, and form the highest level of unimodal processing of acoustic input (Ehret, 1997; Winer and Lee, 2007; King and Schnupp, 2007). In the context of the task, they are involved in sound perception. Although the areas that were observed in this component were also revealed by the regression analysis, interference from ASN in the ICA was smaller than in the GLM. Activity levels were still affected, both in terms of overall component amplitude and stimulus-evoked signal contrast, but the activation extent hardly changed at all. This suggests that even though the auditory cortex is less predictably driven by acoustic input during continuous scanning, it still maintains widespread coherent signal fluctuations. In the rest runs an opposite trend was observed: the auditory component was stronger and more extensive in the continuous runs than in the sparse runs. This suggests that stimulation by ASN drives or at least facilitates coherent fluctuations in the auditory system, for instance by enhancing neural synchrony across the auditory cortex.

Component II had a spatial distribution consistent with the default mode network (Raichle and Snyder, 2007). This network is considered to be involved in introspective and self-referential thought that occurs in the absence of goal-oriented mental activity. Its primary characteristic is that it is generally deactivated by task performance. Indeed, this component was the only one that displayed significant negative responses to the sound presentations, consistent with this interpretation. Moreover, this component's power was larger in the rest runs than in the task runs, similarly pointing to engagement of these areas when no explicit task is performed. In accordance with a previous report (Gaab et al., 2008), the magnitude of the task-induced deactivation (or task-inhibited activation) in the task runs decreased in the presence of ASN. Contrariwise, in the rest runs this component appeared stronger in the presence of ASN. Like for the auditory component, this suggests that ASN reduces evoked responses to other sound stimuli, but at the same time induces coherent fluctuations in brain activity itself.

Component III comprised the superior thalamus and putamen, and roughly represents the basal ganglia. Although the dorsal striatal area is classically regarded to be involved in the regulation of movement, it has also been more generally associated with motivated behavior, including processes related to emotion, reward, and learning (Graybiel, 2005; Hikosaka et al., 2008; Haber and Calzavara, 2009; Pennartz et al., 2009). It has been shown to receive direct corticofugal projections from the auditory cortex (Winer, 2005), and it can be activated by sound (Mitterschiffthaler et al., 2007; Grahn and Rowe, 2009). Together with the thalamic gateways, it is presumably involved in the attentional gating of salient sound stimuli (Campbell et al., 2007). The activity of this component was strongly dependent on task performance, but it was hardly affected by ASN. This suggests that, regardless of stimulus audibility and background ASN, similar attentional resources were recruited and devoted to the task.

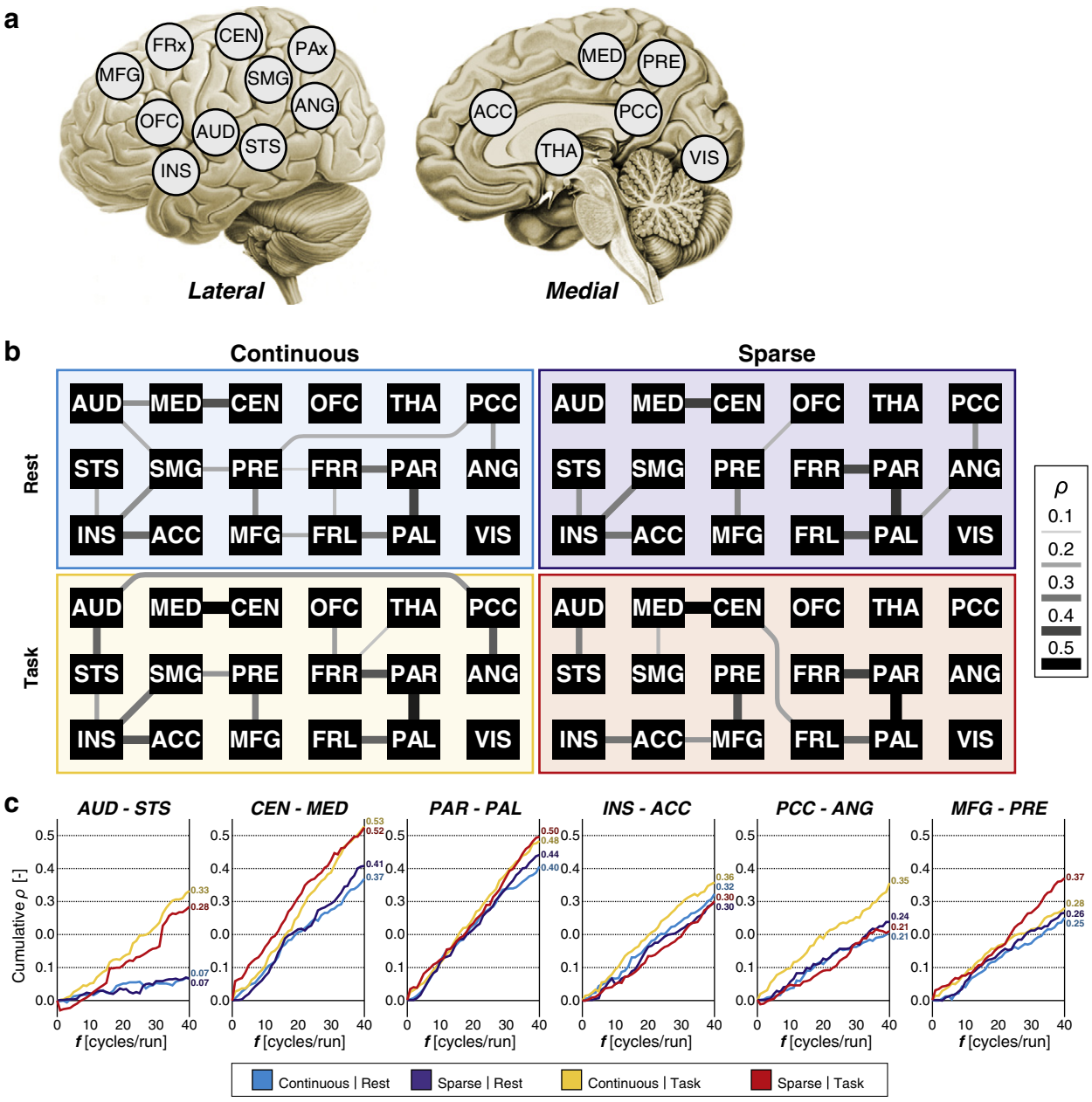

Fig. 7. Effective connectivity model. [a] Eighteen regions of interest (ROIs) were defined, as schematically depicted in these lateral and medial brain views. Frontal (FR*x*) and parietal (PA*x*) ROIs were defined for the left and right hemispheres separately ($x = L/R$). All ROIs are listed in Table 1. [b] A non-causal effective connectivity model was evaluated in which all ROIs potentially connected to all other ROIs. For each of the acquisition methods (continuous or sparse) and each of the behavioral paradigms (rest or task), partial correlation coefficients between all ROIs were calculated. All pairs of ROIs that had significant positive effective connectivity (Bonferroni-corrected $p < 0.05$) are connected by a solid line with a thickness and grayscale level that is proportional to the corresponding partial correlation coefficient ρ. Note that most of the strongest connections were robust across all runs, with the exception of AUD-STS, which was strongly task-related. [c] For six pairs of ROIs, partial correlations were decomposed across frequencies, and cumulative totals were plotted. The value reached at the Nyquist frequency of 40 cycles/run corresponds with the value displayed in panel b.

Component IV primarily comprised the region of the superior temporal sulcus, including the lower bank of the superior temporal gyrus and the upper bank of the middle temporal gyrus. Various roles are attributed to this part of the brain, including social functions like the processing of faces and speech, and theory of mind (Hein and Knight, 2008). In the context of sensory processing, it is commonly regarded as a site of auditory association and multimodal integration (Calvert, 2001). It also forms a likely anatomical substrate of the putative 'what' pathway, which is related to the identification of auditory objects in the subject's environment on the basis of their acoustic features (Griffiths and Warren, 2004; Rauschecker and Tian, 2000). This pathway is thought to project to frontal cortex, and involvement of lateral frontal areas was also present. This component responded to the sound stimuli, but its activity was not detrimentally affected by the presence of ASN. This is consistent with a role in higher-order auditory processing, in which case the neural activity would be less directly related to the acoustic attributes of perceived stimuli per se, but may encode a more abstract representation of a sound source (Engel et al., 2009; Carlyon, 2004). In the brain areas that comprise component IV, ASN may already have been identified as a separate stream of irrelevant acoustic content, the further processing of which may be suppressed in the context of the task.

Weaker and less significant sound- or task-evoked activation was observed in left and right frontal and parietal areas, as well as cingulate and insular cortex (V–VII). These areas have repeatedly been observed to co-activate, and have been grouped into a frontoparietal executive

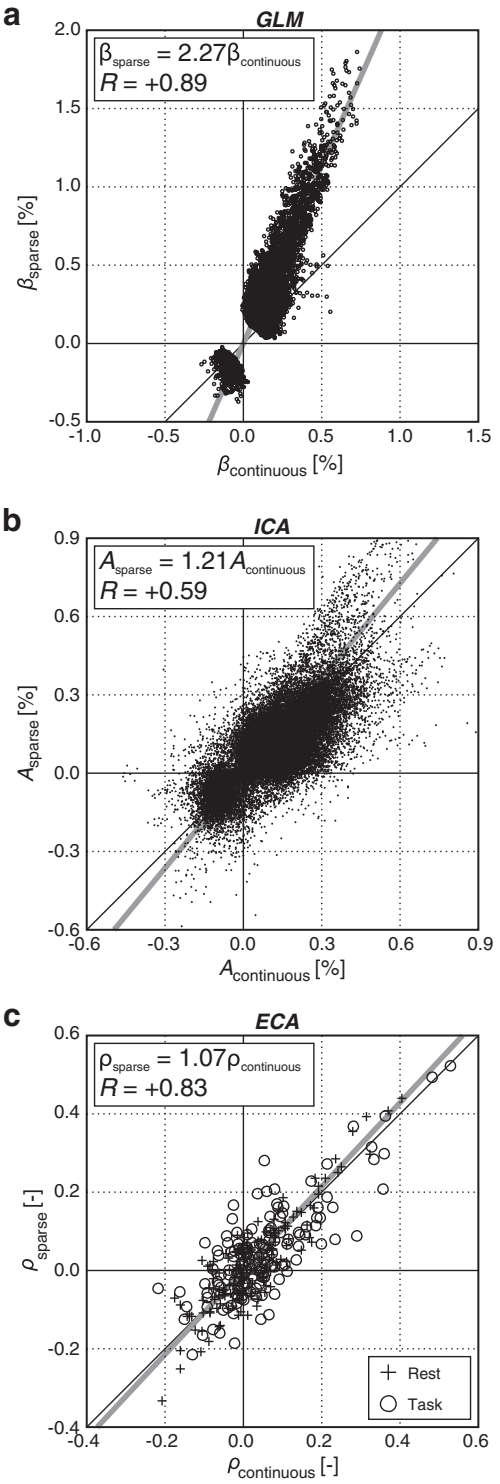

Fig. 8. Primary outcome measures during sparse vs. continuous scanning. Comparisons were made between the outcomes of [a] the general linear model (GLM): the percentages signal change β in all significantly activated voxels; [b] the independent component analysis (ICA): the RMS amplitude A in all voxels that exceeded the imposed threshold in the aggregate data; and [c] the effective connectivity analysis (ECA): all effective connectivity levels ρ between pairs of ROIs, regardless of significance. Each panel displays the sparse outcomes versus the corresponding continuous ones. For the GLM, response magnitudes tended to be larger for sparse sampling (i.e. the slope of the principal axis exceeded 1.0). Contrariwise, the outcomes of the ICA and especially the ECA were only weakly dependent on the acquisition method (i.e. the slope was close to 1.0).

control network and a paralimbic salience network, respectively (Seeley et al., 2007; Dosenbach et al., 2007; Spreng et al., 2010; Menon and Uddin, 2010). Their precise role in the context of the present task can only be speculated on, but may for instance be related to switching between internal and external attention, executive control in relation to the task, emotional associations induced by the sound fragments, memory consolidation, or spatial localization and auditory scene analysis (Bamiou et al., 2003; Tomasi et al., 2005; Sander et al., 2007; Sridharan et al., 2008; Diekhof et al., 2009). Activation levels were too small to confidently assess the effects of acquisition method and interference of ASN in these areas.

Some independent components seemed unaffected by the task. These included the sensorimotor and visual systems (IX–X), which did not play any obvious role in the auditory memory task that was employed. Another example comprised the angular gyrus and posterior cingulate cortex (VIII), which have also been implicated in the default mode network. We did not observe any task-related deactivation in the time course of this component, nor did its power depend upon the presence of a task. This is consistent with a recent report that implicit memory tasks do not disrupt default mode network activity (Yang et al., 2010). Yet, this behavior strongly differed from that of component II, which we consider to be more characteristic for the default mode network. The existence of multiple default mode networks has been coined before (Long et al., 2008; Fox et al., 2005), and the diverging dynamic behavior of the two components in our study does suggest that the dissociation is functionally meaningful. We tentatively hypothesize that the default mode network of component II is involved in 'conscious' internalized mental activity ('thought') that can be suppressed by diverting attentional resources e.g. to a task, whereas the brain areas in component VIII correspond with 'subconscious' internalized mental activity ('awareness') that persists even when performing other tasks.

In addition to stimulus-evoked responses in some of the component time courses, without exception a decrease occurred in spectral power as a function of frequency. In more than half of the components and runs, this spectral decline reached statistical significance. These observations concur with previous reports that resting state connectivity, as measured by BOLD fMRI, is driven by slow oscillations (Cordes et al., 2001; Fransson, 2005; Auer, 2008). We found that the spectral decline was typically stronger in the rest runs than in the task runs. This shows that the dominance of low-frequency fluctuations is not likely caused by processes related to the measurement process itself, but seems to be tied to brain activity. Also, it seems rather specific for resting state.

Interestingly, our results also newly revealed a consistent trend that this spectral decline was stronger in the continuous runs than in the sparse runs. Before we can attribute this finding to differences in neural dynamics, a number of confounding artifacts should be excluded. First, the two sets of fMRI images differ in tissue contrast due to the unequal TR. Although signals were expressed in relative units of percentage signal change, sensitivity to the BOLD contrast may still deviate between the two acquisition types. This conceivably leads to differences in response signal magnitude, and therefore overall spectral power. Such effects would render an absolute comparison of the vertical offsets in Fig. 6 meaningless. However, they would not affect the shape of the spectral profile, including the spectral slope. Second, we did not include any retrospective corrections for e.g. slice timing or physiological signal contributions (i.e., cardiac and respiratory effects) in our processing pipeline. Although such corrections are common and would have been useful for the continuously acquired data, the poor temporal resolution in the sparse runs precludes the required interpolation or filtering of signal time courses. To avoid introducing confounds, we employed identical preprocessing for all data, and also omitted the aforementioned steps in the analysis of the continuously acquired data. This may have led to an elevated noise floor, rendering any effects of interest less detectable, but in our opinion it cannot explain the observed differences

in spectra. Third, one could argue that the spectrum for the sparse acquisitions is flat because of the low sampling rate in the sparse acquisitions. As a result, all signal power at (unobservable) high frequencies is aliased across the (observable) low frequencies. However, because we sub-sampled the continuous data to the same temporal resolution before the spectra were determined, the same would hold for the continuous data. Therefore, aliasing cannot explain the different slopes of the sparse and continuous spectra either. Finally, we argue that it is difficult to conceive how methodological mechanisms related to MR-physics or preprocessing would specifically arise in components that represent various brain systems. Therefore, we conclude that the diverging independent component spectra arise as a result of differences in the underlying neural dynamics.

Given that in 8 out of 10 components of interest the spectral decline was stronger in the continuous than in the sparse runs, our findings suggest that ASN influences the neurodynamics of widespread brain networks. In particular, this influence is not limited to nominally auditory brain regions. The relative importance of slow oscillations that have repeatedly been shown to drive resting state networks is larger during continuous scanning than in the presence of interspersed periods of scanner silence. Either the presence of ongoing ASN contributes to induce slow fluctuations during continuous scanning, or the presence of intermittent ASN decreases spontaneous slow fluctuations during resting state when sparse acquisitions are employed.

So why would slow BOLD signal fluctuations be more salient in the sparse resting state runs than in the continuous runs? It is our experience that the regular ongoing sound that accompanies continuous scanning may eventually achieve a tranquil soothing quality. In fact, in spite of loud ASN, subjects have been known to fall asleep in the MR-scanner when no participation in a task was required. In sharp contrast, and in spite of its periodical nature, the intermittent noise that accompanies sparsely acquired scans retains an alarming and startling effect due to its sudden onsets. We presume that this difference may actually result in subjects being more aroused, wakeful, alert and vigilant during sparse scanning, whereas remaining calm, drowsy, sedate and serene during continuous scanning. This mechanism can explain why the slow fluctuations in spontaneous brain activity that are characteristic of resting state are more pronounced during continuous scanning than during sparse scanning (Boly et al., 2008; He and Raichle, 2009). It would also explain why a low-frequency dominance is absent in task-related runs, irrespective of the acquisition method: in such experiments, subjects remain aroused and wakeful and are required to be alert and vigilant due to the presence of the task itself, and this likely overshadows the effects of scanner noise (except of course for direct interactions with possible acoustic stimuli related to the task). Interestingly, this mechanism has an analogue in electroencephalographic recordings, where the prevalence of slow-wave oscillations (<1 Hz) is associated with non-REM sleep and reduced consciousness (Crunelli and Hughes, 2010; Coenen, 1998). Yet, although we find an explanation in terms of alertness and arousal particularly plausible, we cannot and do not exclude other possible mechanisms.

The interrelations between various regions of interest were studied further by functional and effective connectivity analyses. In the ECA, very strong interactions between AUD and STS were shown in the task runs, but no such interactions existed in the rest runs. This held irrespective of the use of sparse or continuous acquisitions. The functional connectivity outcomes agreed with these observations, in the sense that the connectivity level and extent in the maps related to AUD and STS were higher in the task runs than in the rest runs, but no differences were noted between the continuous and sparse runs. The spectral decompositions of the partial correlation coefficients also showed that differences related to the paradigm were much more influential than differences related to the acquisition method. A task-dependence in the mentioned connectivity patterns is not surprising, since these regions are involved in sound perception and are therefore strongly engaged by the employed task. However, less obvious, the outcomes of the employed connectivity measures were remarkably insensitive to the presence of ASN.

The auditory network (AUD and STS) effectively connected to the salience network (INS and ACC) and, partly via that, to the default mode network (SMG, PRE and MFG). Our results are consistent with a role for the INS in switching attentional resources back and forth between (task-related) external stimulus input and (resting state) internal mental processes (Sridharan et al., 2008). These networks were quite similarly connected in the rest and task continuous runs. In the sparse runs, some of these connections (like SMG-PRE) proved insignificant. Still, overall, the mentioned collection of ROIs (AUD, STS, INS, ACC, SMG, PRE, and MFG) appeared to form a comprehensive 'core network'. The corresponding functional connectivity maps also revealed only weak dependence upon task performance, and no dependence upon acquisition method was observed. These findings again suggest that network interactions are not necessarily more reliably or sensitively detected in the absence of ASN than in its presence.

Various other sub-networks were apparent, like the pair MED–CEN that was always strongly connected, or similarly the pair PCC–ANG. A chain of ROIs FRR–PAR–PAL–FRL formed a robust executive control network (Seeley et al., 2007; Spreng et al., 2010). The remaining ROIs (THA, OFC, and VIS) typically appeared in isolation, and should perhaps be regarded as sub-networks on their own. Connections among these various sub-networks were incidental. In particular, none of these connections appeared in more than one run.

Finally, a direct comparison was made between the effects of ASN on the outcomes of the GLM, ICA, and ECA. Activation levels according to the GLM were strongly dependent on the presence of ASN. Detectable responses in individual activated voxels proved to be reduced approximately twofold. In contrast, the power of ICA components was much less influenced by ASN. A small number of components was affected by the presence of ASN, but many were not. Overall, only a moderate reduction in average component power remained. The ECA connectivity levels were even less sensitive to ASN. With the exception of one pair of ROIs (AUD and STS), none of the connections could be demonstrated to be consistently affected by ASN. Although we do not wish to claim that ASN does not affect network-related brain connectivity methods in any way, our results certainly indicate that effects of ASN are much weaker than for traditional task-related brain activation methods.

Of course, in some applications the presence of ASN might still affect resting state activity in a much more direct fashion. For example, tinnitus patients chronically perceive sound in the absence of any external sound sources (Møller, 2007), and patients that suffer from psychotic disorders like schizophrenia may spontaneously perceive auditory hallucinations (Dierks et al., 1999). Similar percepts can also be induced in healthy subjects following e.g. sleep deprivation or prolonged periods of stress (Asaad and Shapiro, 1986). Furthermore, people may routinely engage in sound-related mental processing during rest, like imagery of sound, memory retrieval of music, or rehearsal of speech (Zatorre, 2007). And finally, a noisy environment may also intrude on other mental processes, especially in subjects with phonophobia, hyperacusis, or information processing disorders like autism (Nieto Del Rincón, 2008). For these examples, the influence of ASN might be larger than we observed in our study. Therefore, ASN should remain an experimental design consideration for particular applications of resting state fMRI.

In summary, we conclude that the use of sparse acquisitions remains strongly advisable for the detection of sound-evoked brain activity by means of conventional regression models. When using blind signal detection methods like ICA as well as functional connectivity measures, sparse acquisitions only provide a moderate advantage, mostly limited to the detection of brain areas directly involved in sound processing. For the extraction of effective connectivity in the brain, any potential advantages of the use of sparse scanning appear negligible. For that

purpose, continuous scanning should mostly be preferred due to its superior temporal resolution. This finding contrasts with our original hypothesis that ASN would affect functional and effective connectivity measures in similar fashion as conventional evoked response measures. However, we did find that low-frequency fluctuations in the BOLD signal are more pronounced in resting state than in stimulated acquisition, and during continuous scanning than during sparse scanning. This suggests that these fluctuations are related to a state of rest or inactivity, and that the ASN from a sparse scanning sequence is more disturbing to this state than noise from a continuous scanning sequence. Thus, ASN forms a pervasive confound in the assessment of brain dynamics during rest.

Funding

This work was supported by The Netherlands Organisation for Scientific Research (NWO) and The Netherlands Organisation for Health Research and Development (ZonMW) through the 'VENI' Innovational Research Incentives Scheme (grant number 016.096.011 to D.L.).

Appendix A. Supplementary data

Supplementary data to this article can be found online at doi:10.1016/j.neuroimage.2011.01.019.

References

Amaro, E., Williams, S.C.R., Shergill, S.S., Fu, C.H.Y., MacSweeney, M., Picchioni, M.M., Brammer, M.J., McGuire, P.K., 2002. Acoustic noise and functional magnetic resonance imaging: current strategies and future prospects. J. Magn. Reson. Imaging 16, 497–510.
Asaad, G., Shapiro, B., 1986. Hallucinations: theoretical and clinical overview. Am. J. Psychiatry 143, 1088–1097.
Auer, D.P., 2008. Spontaneous low-frequency blood oxygenation level-dependent fluctuations and functional connectivity analysis of the 'resting' brain. Magn. Reson. Imaging 26, 1055–1064.
Bamiou, D., Musiek, F.E., Luxon, L.M., 2003. The insula (Island of Reil) and its role in auditory processing. Literature review. Brain Res. Brain Res. Rev. 42, 143–154.
Bandettini, P.A., Jesmanowicz, A., Van Kylen, J., Birn, R.M., Hyde, J.S., 1998. Functional MRI of brain activation induced by scanner acoustic noise. Magn. Reson. Med. 39, 410–416.
Baumgart, F., Kaulisch, T., Tempelmann, C., Gaschler-Markefski, B., Tegeler, C., Schindler, F., Stiller, D., Scheich, H., 1998. Electrodynamic headphones and woofers for application in magnetic resonance imaging scanners. Med. Phys. 25, 2068–2070.
Bell, A.J., Sejnowski, T.J., 1995. An information-maximization approach to blind separation and blind deconvolution. Neural Comput. 7, 1129–1159.
Boly, M., Phillips, C., Tshibanda, L., Vanhaudenhuyse, A., Schabus, M., Dang-Vu, T.T., Moonen, G., Hustinx, R., Maquet, P., Laureys, S., 2008. Intrinsic brain activity in altered states of consciousness: how conscious is the default mode of brain function? Ann. NY Acad. Sci. 1129, 119–129.
Boyle, Y., Bentley, D.E., Watson, A., Jones, A.K.P., 2006. Acoustic noise in functional magnetic resonance imaging reduces pain unpleasantness ratings. Neuroimage 31, 1278–1283.
Calhoun, V.D., Adali, T., Pearlson, G.D., Pekar, J.J., 2001. A method for making group inferences from functional MRI data using independent component analysis. Hum. Brain Mapp. 14, 140–151.
Calvert, G.A., 2001. Crossmodal processing in the human brain: insights from functional neuroimaging studies. Cereb. Cortex 11, 1110–1123.
Campbell, L.E., Hughes, M., Budd, T.W., Cooper, G., Fulham, W.R., Karayanidis, F., Hanlon, M., Stojanov, W., Johnston, P., Case, V., et al., 2007. Primary and secondary neural networks of auditory prepulse inhibition: a functional magnetic resonance imaging study of sensorimotor gating of the human acoustic startle response. Eur. J. Neurosci. 26, 2327–2333.
Carlyon, R.P., 2004. How the brain separates sounds. Trends Cogn. Sci. 8, 465–471 (Regul. Ed.).
Cho, Z.H., Chung, S.C., Lim, D.W., Wong, E.K., 1998. Effects of the acoustic noise of the gradient systems on fMRI: a study on auditory, motor, and visual cortices. Magn. Reson. Med. 39, 331–335.
Coenen, A.M., 1998. Neuronal phenomena associated with vigilance and consciousness: from cellular mechanisms to electroencephalographic patterns. Conscious. Cogn. 7, 42–53.
Cole, D.M., Smith, S.M., Beckmann, C.F., 2010. Advances and pitfalls in the analysis and interpretation of resting-state FMRI data. Front Syst Neurosci 4, 8.
Cordes, D., Haughton, V.M., Arfanakis, K., Carew, J.D., Turski, P.A., Moritz, C.H., Quigley, M.A., Meyerand, M.E., 2001. Frequencies contributing to functional connectivity in the cerebral cortex in "resting-state" data. AJNR Am. J. Neuroradiol. 22, 1326–1333.
Crunelli, V., Hughes, S.W., 2010. The slow (<1 Hz) rhythm of non-REM sleep: a dialogue between three cardinal oscillators. Nat. Neurosci. 13, 9–17.
Damoiseaux, J.S., Rombouts, S.A.R.B., Barkhof, F., Scheltens, P., Stam, C.J., Smith, S.M., Beckmann, C.F., 2006. Consistent resting-state networks across healthy subjects. Proc. Natl. Acad. Sci. U. S. A. 103, 13848–13853.
Diekhof, E.K., Biedermann, F., Ruebsamen, R., Gruber, O., 2009. Top-down and bottom-up modulation of brain structures involved in auditory discrimination. Brain Res. 1297, 118–123.
Dierks, T., Linden, D.E., Jandl, M., Formisano, E., Goebel, R., Lanfermann, H., Singer, W., 1999. Activation of Heschl's gyrus during auditory hallucinations. Neuron 22, 615–621.
Dosenbach, N.U.F., Fair, D.A., Miezin, F.M., Cohen, A.L., Wenger, K.K., Dosenbach, R.A.T., Fox, M.D., Snyder, A.Z., Vincent, J.L., Raichle, M.E., et al., 2007. Distinct brain networks for adaptive and stable task control in humans. Proc. Natl. Acad. Sci. U. S. A. 104, 11073–11078.
Ehret, G., 1997. The auditory cortex. J. Comp. Physiol. A 181, 547–557.
Engel, L.R., Frum, C., Puce, A., Walker, N.A., Lewis, J.W., 2009. Different categories of living and non-living sound-sources activate distinct cortical networks. Neuroimage 47, 1778–1791.
Fox, M.D., Raichle, M.E., 2007. Spontaneous fluctuations in brain activity observed with functional magnetic resonance imaging. Nat. Rev. Neurosci. 8, 700–711.
Fox, M.D., Snyder, A.Z., Vincent, J.L., Corbetta, M., Van Essen, D.C., Raichle, M.E., 2005. The human brain is intrinsically organized into dynamic, anticorrelated functional networks. Proc. Natl. Acad. Sci. U. S. A. 102, 9673–9678.
Fransson, P., 2005. Spontaneous low-frequency BOLD signal fluctuations: an fMRI investigation of the resting-state default mode of brain function hypothesis. Hum. Brain Mapp. 26, 15–29.
Friston, K.J., 1994. Functional and effective connectivity in neuroimaging: a synthesis. Hum. Brain Mapp. 2, 56–78.
Friston, K., 2009. The free-energy principle: a rough guide to the brain? Trends Cogn. Sci. 13, 293–301 (Regul. Ed.).
Friston, K.J., Ashburner, J.T., Kiebel, S.J., Nichols, T.E., Penny, W.D., 2007. Statistical Parametric Mapping: The Analysis of Functional Brain Images, 1st ed. Academic Press.
Fuchino, Y., Sato, H., Maki, A., Yamamoto, Y., Katura, T., Obata, A., Koizumi, H., Yoro, T., 2006. Effect of fMRI acoustic noise on sensorimotor activation examined using optical topography. Neuroimage 32, 771–777.
Gaab, N., Gabrieli, J.D.E., Glover, G.H., 2007. Assessing the influence of scanner background noise on auditory processing. II. An fMRI study comparing auditory processing in the absence and presence of recorded scanner noise using a sparse design. Hum. Brain Mapp. 28, 721–732.
Gaab, N., Gabrieli, J.D.E., Glover, G.H., 2008. Resting in peace or noise: scanner background noise suppresses default-mode network. Hum. Brain Mapp. 29, 858–867.
Grahn, J.A., Rowe, J.B., 2009. Feeling the beat: premotor and striatal interactions in musicians and nonmusicians during beat perception. J. Neurosci. 29, 7540–7548.
Graybiel, A.M., 2005. The basal ganglia: learning new tricks and loving it. Curr. Opin. Neurobiol. 15, 638–644.
Griffiths, T.D., Warren, J.D., 2004. What is an auditory object? Nat. Rev. Neurosci. 5, 887–892.
Grossberg, S., 1999. The link between brain learning, attention, and consciousness. Conscious. Cogn. 8, 1–44.
Haber, S.N., Calzavara, R., 2009. The cortico-basal ganglia integrative network: the role of the thalamus. Brain Res. Bull. 78, 69–74.
Hall, D.A., Haggard, M.P., Akeroyd, M.A., Palmer, A.R., Summerfield, A.Q., Elliott, M.R., Gurney, E.M., Bowtell, R.W., 1999. "Sparse" temporal sampling in auditory fMRI. Hum. Brain Mapp. 7, 213–223.
He, B.J., Raichle, M.E., 2009. The fMRI signal, slow cortical potential and consciousness. Trends Cogn. Sci. 13, 302–309 (Regul. Ed.).
Hein, G., Knight, R.T., 2008. Superior temporal sulcus—it's my area: or is it? J. Cogn. Neurosci. 20, 2125–2136.
Hikosaka, O., Bromberg-Martin, E., Hong, S., Matsumoto, M., 2008. New insights on the subcortical representation of reward. Curr. Opin. Neurobiol. 18, 203–208.
Horwitz, B., Warner, B., Fitzer, J., Tagamets, M., Husain, F.T., Long, T.W., 2005. Investigating the neural basis for functional and effective connectivity. Application to fMRI. Philos. Trans. R. Soc. Lond. B Biol. Sci. 360, 1093–1108.
King, A.J., Schnupp, J.W.H., 2007. The auditory cortex. Curr. Biol. 17, R236–R239.
Lancaster, J.L., Woldorff, M.G., Parsons, L.M., Liotti, M., Freitas, C.S., Rainey, L., Kochunov, P.V., Nickerson, D., Mikiten, S.A., Fox, P.T., 2000. Automated Talairach atlas labels for functional brain mapping. Hum. Brain Mapp. 10, 120–131.
Langers, D.R.M., 2010. Unbiased group-level statistical assessment of independent component maps by means of automated retrospective matching. Hum. Brain Mapp. 31, 727–742.
Langers, D.R.M., van Dijk, P., Backes, W.H., 2005a. Lateralization, connectivity and plasticity in the human central auditory system. Neuroimage 28, 490–499.
Langers, D.R.M., Van Dijk, P., Backes, W.H., 2005b. Interactions between hemodynamic responses to scanner acoustic noise and auditory stimuli in functional magnetic resonance imaging. Magn. Reson. Med. 53, 49–60.
Long, X., Zuo, X., Kiviniemi, V., Yang, Y., Zou, Q., Zhu, C., Jiang, T., Yang, H., Gong, Q., Wang, L., et al., 2008. Default mode network as revealed with multiple methods for resting-state functional MRI analysis. J. Neurosci. Meth. 171, 349–355.
López-Ibor, J.J., López-Ibor, M., Pastrana, J.I., 2008. Transcranial magnetic stimulation. Curr. Opin. Psychiatry 21, 640–644.
Maldjian, J.A., Laurienti, P.J., Kraft, R.A., Burdette, J.H., 2003. An automated method for neuroanatomic and cytoarchitectonic atlas-based interrogation of fMRI data sets. Neuroimage 19, 1233–1239.
Marrelec, G., Krainik, A., Duffau, H., Pélégrini-Issac, M., Lehéricy, S., Doyon, J., Benali, H., 2006. Partial correlation for functional brain interactivity investigation in functional MRI. Neuroimage 32, 228–237.
Mayer, A.R., Hanlon, F.M., Franco, A.R., Teshiba, T.M., Thoma, R.J., Clark, V.P., Canive, J.M., 2009. The neural networks underlying auditory sensory gating. Neuroimage 44, 182–189.

Menon, V., Uddin, L.Q., 2010. Saliency, switching, attention and control: a network model of insula function. Brain Struct. Funct. 214, 655–667.
Mitterschiffthaler, M.T., Fu, C.H.Y., Dalton, J.A., Andrew, C.M., Williams, S.C.R., 2007. A functional MRI study of happy and sad affective states induced by classical music. Hum. Brain Mapp. 28, 1150–1162.
Moelker, A., Pattynama, P.M.T., 2003. Acoustic noise concerns in functional magnetic resonance imaging. Hum. Brain Mapp. 20, 123–141.
Møller, A.R., 2007. Tinnitus: presence and future. Prog. Brain Res. 166, 3–16.
Nieto Del Rincón, P.L., 2008. Autism: alterations in auditory perception. Rev. Neurosci. 19, 61–78.
Oldfield, R.C., 1971. The assessment and analysis of handedness: the Edinburgh inventory. Neuropsychologia 9, 97–113.
Pennartz, C.M.A., Berke, J.D., Graybiel, A.M., Ito, R., Lansink, C.S., van der Meer, M., Redish, A.D., Smith, K.S., Voorn, P., 2009. Corticostriatal interactions during learning, memory processing, and decision making. J. Neurosci. 29, 12831–12838.
Raichle, M.E., Snyder, A.Z., 2007. A default mode of brain function: a brief history of an evolving idea. Neuroimage 37, 1083–1090 discussion 1097–1099.
Rauschecker, J.P., Tian, B., 2000. Mechanisms and streams for processing of "what" and "where" in auditory cortex. Proc. Natl. Acad. Sci. U. S. A. 97, 11800–11806.
Robertson, J.A., Théberge, J., Weller, J., Drost, D.J., Prato, F.S., Thomas, A.W., 2010. Low-frequency pulsed electromagnetic field exposure can alter neuroprocessing in humans. J. R. Soc. Interface 7, 467–473.
Rogers, B.P., Morgan, V.L., Newton, A.T., Gore, J.C., 2007. Assessing functional connectivity in the human brain by fMRI. Magn. Reson. Imaging 25, 1347–1357.
Rohan, M., Parow, A., Stoll, A.L., Demopulos, C., Friedman, S., Dager, S., Hennen, J., Cohen, B.M., Renshaw, P.F., 2004. Low-field magnetic stimulation in bipolar depression using an MRI-based stimulator. Am. J. Psychiatry 161, 93–98.
Sander, K., Frome, Y., Scheich, H., 2007. FMRI activations of amygdala, cingulate cortex, and auditory cortex by infant laughing and crying. Hum. Brain Mapp. 28, 1007–1022.
Scarff, C.J., Dort, J.C., Eggermont, J.J., Goodyear, B.G., 2004. The effect of MR scanner noise on auditory cortex activity using fMRI. Hum. Brain Mapp. 22, 341–349.
Schöpf, V., Kasess, C.H., Lanzenberger, R., Fischmeister, F., Windischberger, C., Moser, E., 2010. Fully exploratory network ICA (FENICA) on resting-state fMRI data. J. Neurosci. Meth. 192, 207–213.
Seeley, W.W., Menon, V., Schatzberg, A.F., Keller, J., Glover, G.H., Kenna, H., Reiss, A.L., Greicius, M.D., 2007. Dissociable intrinsic connectivity networks for salience processing and executive control. J. Neurosci. 27, 2349–2356.
Smith, A.M., Lewis, B.K., Ruttimann, U.E., Ye, F.Q., Sinnwell, T.M., Yang, Y., Duyn, J.H., Frank, J.A., 1999. Investigation of low frequency drift in fMRI signal. Neuroimage 9, 526–533.
Smith, S.M., Fox, P.T., Miller, K.L., Glahn, D.C., Fox, P.M., Mackay, C.E., Filippini, N., Watkins, K.E., Toro, R., Laird, A.R., et al., 2009. Correspondence of the brain's functional architecture during activation and rest. Proc. Natl. Acad. Sci. U. S. A. 106, 13040–13045.
Spreng, R.N., Stevens, W.D., Chamberlain, J.P., Gilmore, A.W., Schacter, D.L., 2010. Default network activity, coupled with the frontoparietal control network, supports goal-directed cognition. Neuroimage 53, 303–317.
Sridharan, D., Levitin, D.J., Menon, V., 2008. A critical role for the right fronto-insular cortex in switching between central-executive and default-mode networks. Proc. Natl. Acad. Sci. U. S. A. 105, 12569–12574.
Talavage, T.M., Edmister, W.B., Ledden, P.J., Weisskoff, R.M., 1999. Quantitative assessment of auditory cortex responses induced by imager acoustic noise. Hum. Brain Mapp. 7, 79–88.
Tomasi, D., Caparelli, E.C., Chang, L., Ernst, T., 2005. fMRI-acoustic noise alters brain activation during working memory tasks. Neuroimage 27, 377–386.
Winer, J.A., 2005. Decoding the auditory corticofugal systems. Hear. Res. 207, 1–9.
Winer, J.A., Lee, C.C., 2007. The distributed auditory cortex. Hear. Res. 229, 3–13.
Woods, D.L., Stecker, G.C., Rinne, T., Herron, T.J., Cate, A.D., Yund, E.W., Liao, I., Kang, X., 2009. Functional maps of human auditory cortex: effects of acoustic features and attention. PLoS ONE 4, e5183.
Yang, J., Weng, X., Zang, Y., Xu, M., Xu, X., 2010. Sustained activity within the default mode network during an implicit memory task. Cortex 46, 354–366.
Zatorre, R.J., 2007. There's more to auditory cortex than meets the ear. Hear. Res. 229, 24–30.
Zhang, N., Zhu, X., Chen, W., 2005. Influence of gradient acoustic noise on fMRI response in the human visual cortex. Magn. Reson. Med. 54, 258–263.